applied sciences

MDPI

Article

Dynamic Dark Channel Prior Dehazing with Polarization

Haotong Suo [1], Jinge Guan [1,2,*], Miao Ma [3], Yongsheng Huo [1], Yaoyu Cheng [1], Naying Wei [4] and Liying Zhang [4]

[1] School of Information and Communication Engineering, North University of China, Taiyuan 030051, China; htsuo@st.nuc.edu.cn (H.S.); zbdx_hys@163.com (Y.H.); chengyaoyu66@163.com (Y.C.)
[2] State Key Laboratory of Dynamic Measurement Technology, Taiyuan 030051, China
[3] Department of Science, Taiyuan Institute of Technology, Taiyuan 030008, China; mam@tit.edu.cn
[4] School of Instrument and Electronics, North University of China, Taiyuan 030051, China; weiny2867@163.com (N.W.); lyzhang@st.nuc.edu.cn (L.Z.)
* Correspondence: jgguan@nuc.edu.cn

Abstract: For traditional dark channel prior (DCP) imaging through haze environments, intensity information acts as the carrier to acquire the reflective character of the dehazed target image. We introduce polarization as auxiliary information into the traditional DCP dehazed process for achieving better imaging performance that can improve target detection or target tracking. In this paper, a polarization imaging system with a split-amplitude structure is designed to enable real-time polarization acquisition of transient scenes. The experimental results show that besides descattering, the proposed method can also simultaneously obtain both light intensity and polarization information from the target. Compared with the traditional DCP method, which only utilizes intensity information as a carrier, a combination of intensity and polarization in the proposed method can effectively detect the target hidden in the background with similar reflectivity. Our investigation has potential application value for optical imaging in scattering environments.

Keywords: dark channel prior; polarization; target detection

check for updates

Citation: Suo, H.; Guan, J.; Ma, M.; Huo, Y.; Cheng, Y.; Wei, N.; Zhang, L. Dynamic Dark Channel Prior Dehazing with Polarization. *Appl. Sci.* **2023**, *13*, 10475. https://doi.org/10.3390/app131810475

Academic Editor: Andrea Prati

Received: 2 August 2023
Revised: 16 September 2023
Accepted: 18 September 2023
Published: 19 September 2023

Copyright: © 2023 by the authors. Licensee MDPI, Basel, Switzerland. This article is an open access article distributed under the terms and conditions of the Creative Commons Attribution (CC BY) license (https://creativecommons.org/licenses/by/4.0/).

1. Introduction

In hazy weather conditions, conventional optical imaging systems are disturbed by a large number of suspended particles in the air, and the scattering and absorption effects of these suspended particles on light can lead to reduced visibility [1]. In turn, this makes the detection distance, imaging effect and measurement accuracy of the imaging system substantially limited, thus seriously affecting the target imaging effect, and the acquisition of key parameters [2]. To suppress the influence of light scattering effects on the imaging process, many researchers have conducted various studies on image dehazing.

In the past few decades, many image dehazing methods have been developed. These methods can be roughly divided into single-image dehazing and multi-image dehazing according to the number of images used in the dehazing process. Single-image dehazing mainly deals with a single hazy image and enhances or restores the image quality by processing the image captured by the optical system. Some examples of single-image dehazing techniques are histogram equalization [3], wavelet transform [4], and the prior-based dehazing technique proposed by He et al. [5–7]. These methods are usually used to process the acquired images, which perform well in target detection, but their shortcomings of using light intensity information as a carrier and having a single optical dimension lead to a decrease in the effectiveness of their target characterization [8].

Multi-image dehazing mainly utilizes the different polarization characteristics of target scattering light and atmospheric scattering light in the image and obtains polarimetric images by using the polarization difference technique. Based on the atmospheric physical scattering model, the image is dehazed, which can effectively improve the clarity and contrast of the target. In this category of methods, the polarization dehazing method has

been proven to be an effective method to improve the quality of blurred images [9–12]. As an important property of light [13], polarization presents unique advantages in the fields of target detection [14], image enhancement under harsh conditions [15], and navigation [16]. Compared with conventional images acquired based on the reflected intensity information, polarization can characterize the vector nature of light waves related to objects in the scene, which provides additional information to improve detection performance.

This paper mainly studies the dark channel prior dehazing method, which has a simple and easy theoretical process and is still a hot topic in the field of dehazing. This paper proposes to introduce polarization information into the traditional dark channel prior to dehazing to enhance discrimination between different objects by taking advantage of the sensitivity of polarization to physical properties. At present, similar methods are discussed in published articles. Chen et al. [17] studied the theory of de-scattering and polarization detection in the dark channel prior to the dehazing method and built a mechanical polarization filtering imaging device. He experimentally verified the target characterization function of the proposed method in a foggy environment. The experimental results showed that while the target contrast was enhanced, the image noise also became more obvious, and the polarization degree image had color distortion. Jia et al. [18] also called it the polarization dark channel prior (PDCP) method. The author mainly applies this method to the enhancement of marine targets. However, the imaging system in this paper has insufficient stability, and if the imaging system has errors or drifts, it will affect the extraction of polarization information and the dehazing effect. In addition, the experimental scene in this paper has strong reflections and highlights, which may interfere with the polarization information. Meng et al. [19] addressed the inaccuracy of the atmospheric light estimation in relation to the dark channel prior theory. They proposed the dark channel quartering to estimate the atmospheric light intensity. This method allows them to simultaneously recover fog-free, high-quality polarization images and scene depth maps from dual images. However, this method is computationally expensive and slow. Moreover, most of the existing dehazing methods based on polarization and dark channel prior are only suitable for static scenes and may not be applicable to dynamic scenes, lacking practical significance.

To address the above problems, this paper developed an intensity-polarization dual-source information dehazing imaging system for dynamic scenes, which is based on a multi-sensor synchronous co-optical path structure and has the function of high-resolution detection compatible with time and space (10 FPS, 1024 × 1024 array). At the same time, different imaging channels can independently acquire the specific polarization state (0°, 45°, 90°, 135°) information of the same transient scene, thus having the ability to output the linear polarization element in the dynamic Stokes vector. Finally, the proposed intensity-polarization dual-source dark channel dehazing system is applied to foggy environments under different weather conditions, and its target detection and identification capabilities are evaluated.

2. Theoretical Analysis

2.1. Principle of Dark Channel Prior Dehazing

The dark channel prior method relies on the atmospheric scattering model for the process of dehazing [20], as shown in Figure 1.

In this model, the influence of the scattering effect on the imaging can be described as follows:

$$I(x) = J(x)t(x) + A(1 - t(x)), \tag{1}$$

where $I(x)$ is the foggy image, $J(x)$ represents the fog-free image, A indicates the intensity of global atmospheric light, x is the spatial position of the pixel, and $t(x)$ is the transmittance with the following expression:

$$t(x) = e^{-rd(x)}, \tag{2}$$

where r represents the atmospheric scattering coefficient and d is the depth of the scene light field.

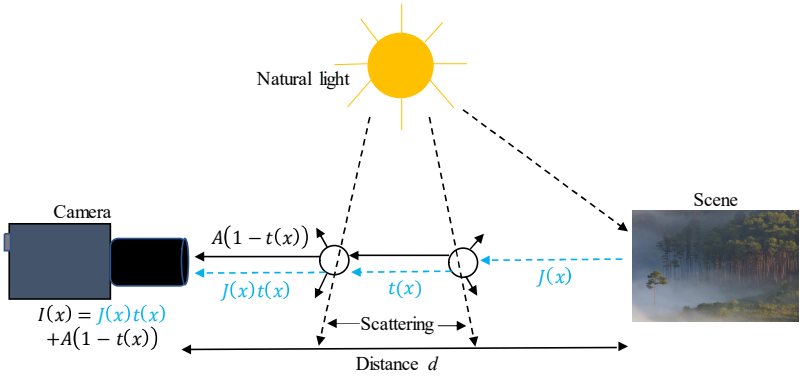


Figure 1. Atmospheric scattering model.

From Figure 1 and Equation (1), the incoherent superposition of direct transmission and atmospheric scattering light is what the optical imaging system ultimately achieves [21].

By observing and summarizing outdoor foggy images, He et al. [22] found the existence of dark channels in the image and proposed a dehazing method based on dark channels. In most local areas (excluding the sky), the intensities of some pixels (called 'dark pixels') in at least one color (RGB) channel are very low and can approach zero.

$$J^{dark}(x) = \min_{y\in\Omega(x)}(\min_{c\in\{r,g,b\}} J^c(y)) \sim 0. \tag{3}$$

The top 0.1% of pixels with the highest intensity are located in the dark channel image and matched in the hazy image. The brightest pixel among the matched ones is chosen as the estimated value of the atmospheric light. Equation (1) is normalized with the estimated value.

$$\frac{I^c(x)}{A^c} = t(x)\frac{J^c(x)}{A^c} + (1 - t(x)), \tag{4}$$

$t(x)$ is simplified as a constant to $\widetilde{t}(x)$, and the minimum value of both sides of Equation (4) is taken twice to obtain the following Equation (5)

$$\min_{y\in\Omega(x)}(\min_c \frac{I^c(x)}{A^c}) = \widetilde{t}(x)\min_{y\in\Omega(x)}(\min_c \frac{I^c(y)}{A^c}) + (1 - \widetilde{t}(x)). \tag{5}$$

Based on the principle of dark channel prior, the estimated value of the transmittance can be calculated as:

$$\widetilde{t}(x) = 1 - \min_{y\in\Omega(x)}(\min_c \frac{J^c(y)}{A^c}). \tag{6}$$

In real-life scenarios, even on fog-free days, there are still some particles suspended in the air. Therefore, the presence of thin fog is still perceived when people are observing distant objects. Moreover, a certain degree of fog adds depth information to the image. It is necessary to preserve a small amount of fog when defogging. A factor of $\omega = 0.95$ is introduced to make the defogged more consistent with human visual perception. The modified formula is shown as follows:

$$\widetilde{t}(x) = 1 - \omega\min_{y\in\Omega(x)}(\min_c \frac{J^c(y)}{A^c}). \tag{7}$$

The premise of the above inference is that the atmospheric light value A is known. He et al. [22] proposed that the value of atmospheric light can be estimated based on the dark channel image. The pixels with gray values in the top 0.1% are found in the dark channel image. Then, the gray value of the pixel with the maximum gray value in the original foggy image $I(x)$ at the corresponding position is taken as the value of A.

Given the transmittance and the value of atmospheric light, the dehazed image can be formulated as:

$$J(x) = \frac{I(x) - A}{t(x)} + A. \tag{8}$$

In addition, to avoid overexposure of the restored image $J(x)$ due to the small values of the transmittance, a threshold $t_0 = 0.1$ is introduced for correction. The final dehazed image formula is written as:

$$J(x) = \frac{I(x) - A}{\max(t(x), t_0)} + A. \tag{9}$$

2.2. Polarization Detection Theory

According to the Fresnel reflection law [23], the object's own properties (such as surface morphology, texture, water content, dielectric constant, and incident angle) determine its characteristic polarization. Using the sensitivity of polarization to physical properties can strengthen the target characteristics, which is conducive to target recognition.

The polarization state of light is usually characterized by the Stokes vector:

$$\mathrm{S} = \begin{bmatrix} S_0 \\ S_1 \\ S_2 \\ S_3 \end{bmatrix} = \begin{bmatrix} \frac{1}{2}(i_0 + i_{45} + i_{90} + i_{135}) \\ i_0 - i_{90} \\ i_{45} - i_{135} \\ i_r - i_l \end{bmatrix}, \tag{10}$$

S_0 is the intensity of the scene total light, S_1 indicates the difference between 0° and 90° polarizations, S_2 represents the difference between 45° and 135° polarizations, S_3 denotes the difference between right-handed and left-handed polarizations, and i means the polarization detection channel.

Under natural conditions, the Stokes vector can be simplified to a vector with only linear polarization components S_0, S_1 and S_2 as the circular polarization characteristics are negligible. The light wave is measured for its polarization information, and the linear polarization degree image *DoLP* is used for visualization. We can use the Stokes vector to measure the linear polarization degree of the scene, which indicates the ratio of polarized components in the total radiance of the scene. The formula for calculating the linear polarization degree (Equation (11)) is as follows:

$$DoLP = \frac{1}{S_0}\sqrt{S_1^2 + S_2^2}. \tag{11}$$

2.3. Polarization-Based Dark Channel Prior Dehazing Method

According to the polarization detection theory in Section 2.2, the total light intensity received by the imaging system can be decomposed into two mutually orthogonal polarization components [6], which are denoted as $I_{\parallel}$ and $I_{\perp}$. The intensity of total light can be written as:

$$I = I_{\parallel} + I_{\perp}, \tag{12}$$

where $I_{\parallel}$ and $I_{\perp}$ represent a set of mutually orthogonal components.

On the basis of the above theory, the atmospheric scattering physical model in Equation (1) is further given by:

$$I_{\parallel}(x) + I_{\perp}(x) = (J_{\parallel}(x) + J_{\perp}(x))t(x) + (A_{\parallel} + A_{\perp})(1 - t(x)). \tag{13}$$

The orthogonal polarization components are derived from the same scene and are independent of each other. Based on Equation (13), the characteristic information of each polarization channel can be further extracted by the following:

$$I_i(x) = J_i(x)t(x) + A_i(1 - t(x)), \tag{14}$$

where i is orthogonal polarization channels.

Based on the theoretical analysis, the images of the original scene are collected in the polarization channels of 0°, 45°, 90°, and 135° and are individually dehazed by the dark channel prior. The processed images retain the polarization information, which is further combined with the polarization theory to detect different targets.

3. Experimental Setup

3.1. Polarization Imaging System

A polarization imaging system with a split-amplitude structure is designed in this paper, which consists of optomechatronics integration.

3.1.1. Optical Module

A cascade prism is used as the beam splitter, which distributes the light from the scene to different detection channels [24], as shown in Figure 2a. The same type of CMOS camera is placed in each detection channel for imaging, and a polarization state analyzer is configured in each of them. Here, only the linearly polarized elements in the Stokes vector are considered, and therefore the orientation of the polarization axis of the polarization state analyzer in each detection channel is set to 0°, 45°, 90°, and 135°, respectively. The physical object of the cascaded beam splitter is shown in Figure 2b. Compared with the traditional discrete beam splitter shown in Figure 2c, the cascaded beam splitter is an integrated device that can effectively avoid the influence of the reflection phenomenon between the prism surfaces on the imaging process and facilitate the coaxial alignment of the prism.

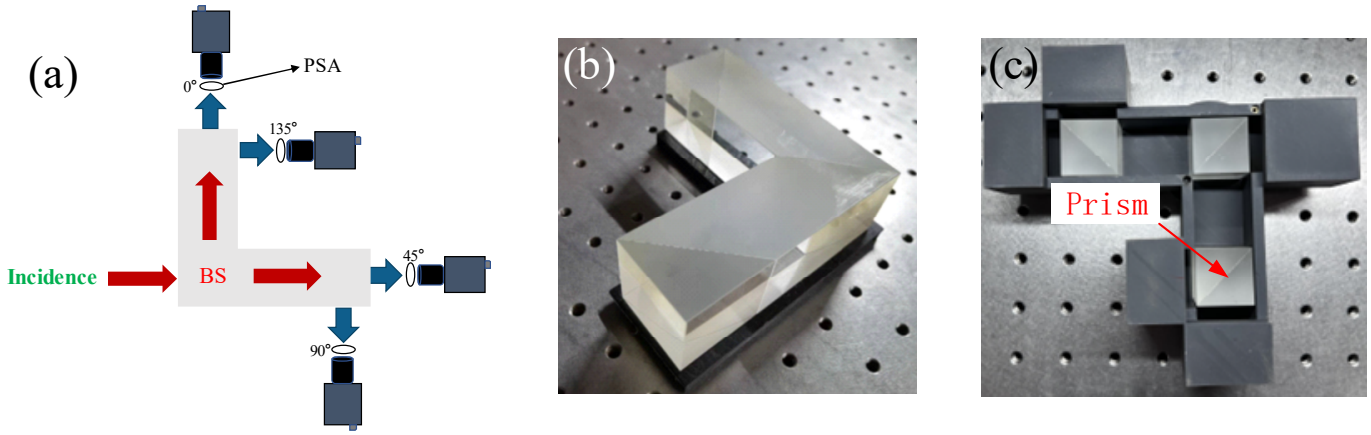


Figure 2. (**a**) Imaging principle. BS: beam splitter; PSA: polarization state analyzer. (**b**) Integrated beam splitter prism. (**c**) Traditional discrete beam splitter.

3.1.2. Mechanical Module

The three-dimensional mechanical structure, which is designed by using of SOLIDWORKS 2018 to fix and arrange optical elements, is made of 8 mm thick aviation aluminum with high strength, corrosion resistance, and oxidation resistance characteristics [25]. This could effectively prevent the damage of the harsh external environment to the optical elements. A three-dimensional adjustment frame was configured in the mechanical structure, which could further enhance the registration degree between different polarimetric imaging units. Figure 3a shows the three-dimensional model of the mechanical module, and Figure 3b represents the structural diagram of the instrument.

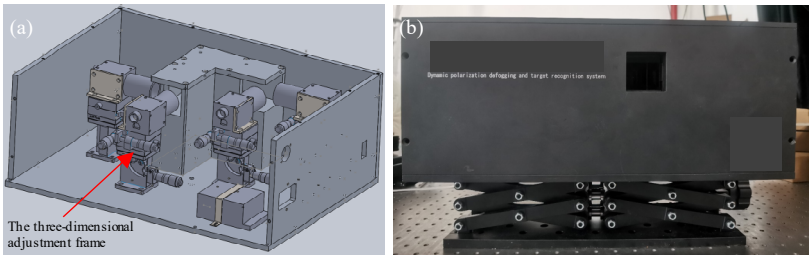


Figure 3. (**a**) The three-dimensional model of the mechanical module. (**b**) The structural diagram of the instrument.

3.1.3. Circuit Module

This paper uses an FPGA chip as the circuit module of the polarization imaging system because FPGAs can process logic signals in parallel. The FPGA used in this paper is Xilinx Spartan-6 series FPGA chip, which is modeled as shown in Figure 4a. The goal of this paper is to independently acquire the specific polarization state (0°, 45°, 90°, 135°) information of the same transient scene in different imaging channels. Therefore, by means of the FPGA, the data in the four polarization channels can be collected in real time, which enables the polarization imaging system to output the linear polarization elements of the dynamic Stokes vector.

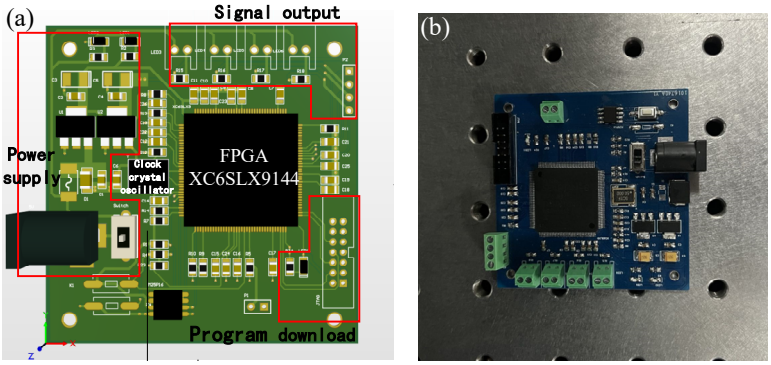


Figure 4. (**a**) Chip model. (**b**) Synchronization control unit.

Design a synchronous trigger circuit based on the Xilinx Spartan-6 series FPGA chip, the corresponding Synchronization control unit is shown in Figure 4b. The different voltages required for the normal operation of the FPGA chip are obtained by converting the 5 V voltage. A linear regulated power supply is selected as the board-level power supply module, which has low ripple and can ensure the stability and reliability of the synchronous control circuit. The LM1117S series LDO buck chip is used to reduce the 5 V to 3.3 V and 1.2 V, and with decoupling capacitors, it can achieve stable and high-quality power output. Based on the FPGA, a synchronous pulse signal generator is designed. In the synchronous control circuit, a 50 MHz crystal oscillator is used to provide a clock signal with a clock cycle of 20 ns. The program download adopts the JTAG communication protocol and uses a Flash chip with a capacity of 16 Mbit to store the program file, which is M25SP16. When the single-board circuit is connected to the power supply, the FPGA chip reads the program from Flash and runs by itself. A counter is defined inside the FPGA, which counts according to the clock frequency. By adjusting the parameters, signals with different pulse widths and different pulse periods can be realized. Since the FPGA is a parallel processing logic device, four pulse signals can be output simultaneously.

3.2. Polarization Axis Calibration System

In order to reduce the influence of polarization filtering errors on imaging accuracy, the axis of the polarization state analyzer needs to be calibrated. The schematic diagram of its principle is shown in Figure 5a. When linearly polarized light passes through a polarizer,

the physical interaction process between them can be quantitatively described by Malus's law [25]:

$$I = I_0 \cos^2 \theta, \tag{15}$$

where I and I_0 are the transmitted and incident light intensities, respectively, and θ is the angle between the vibration direction of the incidence vector and the polarization axis orientation of the polarizer. According to Equation (15), when θ equals to 90° and θ equals to 0°, the transmitted light intensity is minimal and maximal, respectively.

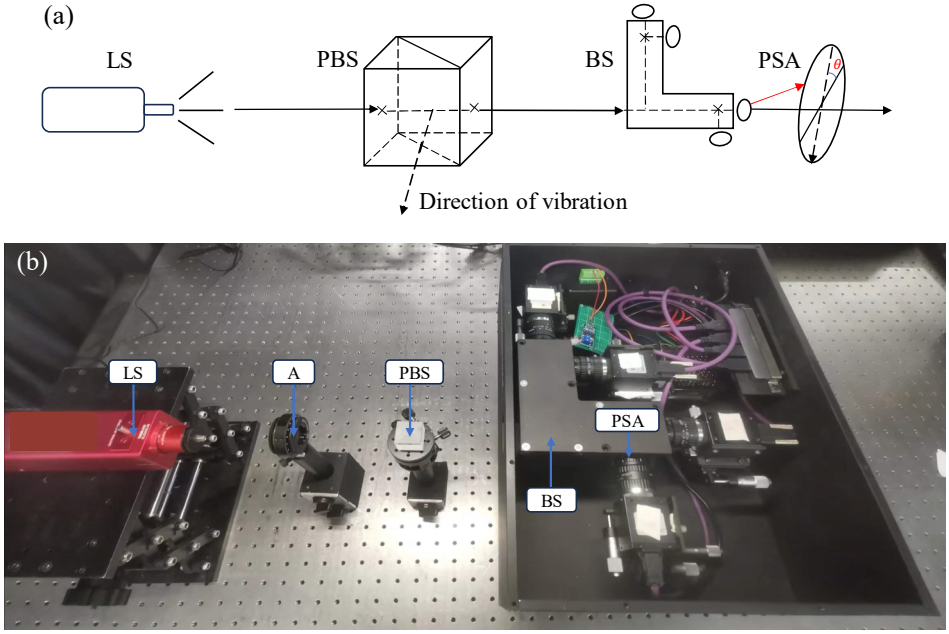


Figure 5. Polarization axis calibration system. (**a**) Schematic diagram. (**b**) System optical path. LS: light source; A: attenuator; PBS: polarization beam splitter; BS: beam splitter; PSA: polarization state analyzer.

On the basis of the above-mentioned theory, the experimental setup for measuring the polarization axis of the polarizer is shown in Figure 5b. A halogen-tungsten lamp is used as the light source in the experiment. Light passing through the polarized beam splitter (PBS) based on the prism is decomposed into two linearly polarized beams: A beam of linearly polarized light enters a cascade prism along its propagation direction, while another beam of linearly polarized light has its electric field vector oscillating perpendicular to its direction of propagation. The linearly polarized light entering the cascade prism is divided into four detection channels, each equipped with a CMOS camera with a polarizer. Next, we calibrate the angles of the four polarizers.

Firstly, we calibrate the 0° and 90° of the PSA by manually rotating two of them. Based on Malus's law, when the angle between the polarization axis of the rotated polarizer and the polarization direction of the incident light is 0°, the light intensity imaged on the CMOS camera through the polarizer is maximized, and thus one polarizer's angle can be determined as 0°. Similarly, when the light intensity imaged on the CMOS camera through the polarizer is minimized, another PSA's angle can be determined as 90°. Then, we rotate the scales on the other two polarizers by 45°, respectively, based on the calibrated 0° and 90°, and thus the PSA's 45° and 135° can be determined.

4. Experimental Results and Discussion

4.1. Polarization Axis Calibration

The relationship between light intensities recorded by the CMOS camera and the orientation of the polarization axis is shown in Figure 6. Here, the orientation range of the polarization axis varies from the formal 0° to 180°, with an interval of 5° related to the

horizontal direction. In order to reduce the artificial error caused by rotating the polarizer, the light intensity corresponding to each polarization axis orientation is measured three times, and the average value of them is taken as the final intensity in the curve. The obtained data is fitted by the Fourier series process. It can be observed that the light intensity achieves the maximum value of 10.1 at the polarization axis of 35° and the minimum value of 2.8 at the polarization axis of 125°, which correspond to the horizontal and vertical directions of the polarization axis, respectively.

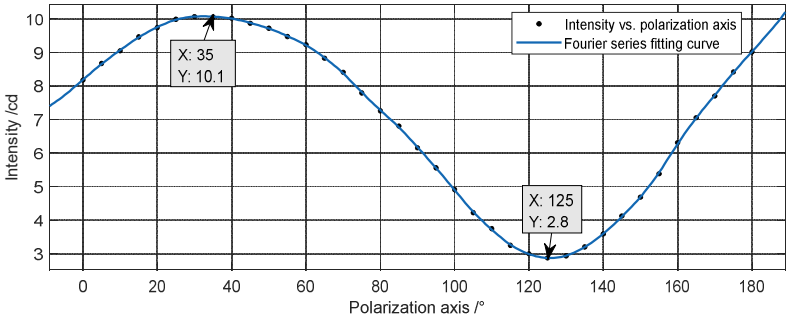


Figure 6. The fitting curve of the relationship between light intensity and the polarization axis.

4.2. Polarization-Based Dark Channel Prior Processing

During the experiment, multiple frames of foggy images were collected from each polarization detection channel. Figure 7a presents the original polarization images of 0°, 45°, 90°, and 135° at a certain time, subsequently referring to the horizontal direction. It can be observed that the quality of all polarization images is severely degraded due to the effect of scattering light component originating from suspended atmospheric particles, which is imaged as noise. Figure 7b further provides the corresponding polarization images processed by the dark channel prior dehazing method. By comparing Figure 7a with Figure 7b, the dark channel prior dehazing method can improve the image contrast by suppressing the impact of the scattering effect on the imaging process.

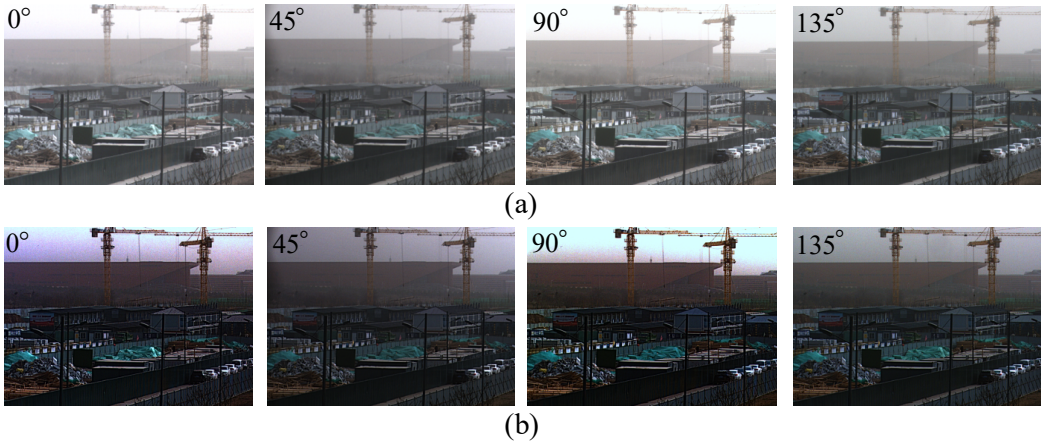


Figure 7. Different polarization channels for (**a**) original images and (**b**) dehazing images processed by the dark channel prior.

In order to demonstrate the performance of polarization in improving target detection and recognition efficiency, a comparison imaging effect between the original, the dark channel prior, and the polarization-based dark channel prior images of the scene is conducted. In the original imaging condition, it is difficult to discriminate the objects from each other within the rectangular regions of 1, 2, and 3 in the image, as shown in Figure 8a. It could be attributed to the superposition of scattering light components on the fog-free image. In the dark channel prior to the imaging condition, the scene could be identified clearly due to the

removal of scattering light, as shown in Figure 8b. However, the traditional dark channel prior method uses intensity information as a carrier to describe the scene. As a result, it is hard to differentiate the target from its background with similar reflectivity, as presented in the designated rectangular regions. When the polarization is further used, the contrast between the target and the background in the designated rectangular regions is significantly improved, as shown in Figure 8c. This could be explained by the fact that polarization information is encoded by the polarization-based dark channel prior dehazing method using the degree of linear polarization. The obvious difference in polarization information between the target and the background allows them to be clearly identified from each other. This also provides a scientific basis to physically enhance the target features in foggy environments through the use of polarization information.



Figure 8. A detailed comparison of different image processing schemes. (**a**) The original scene image. (**b**) The scene image is processed by the dark channel prior to the dehazing method. (**c**) The scene image obtained through the polarization-based dark channel prior dehazing method.

In order to make a more objective evaluation of the effects of image processing, we take advantage of the non-reference image quality metric, the natural image quality evaluator (NIQE), to evaluate the results of image processing. According to the definition of NIQE, a lower NIQE indicates that an image has better quality. The NIQE of each scheme is summarized in Table 1 for comparison. Table 1 shows that the NIQE of the recovered images by PDCP is the lowest. Therefore, the quality of the images by PDCP is the highest.

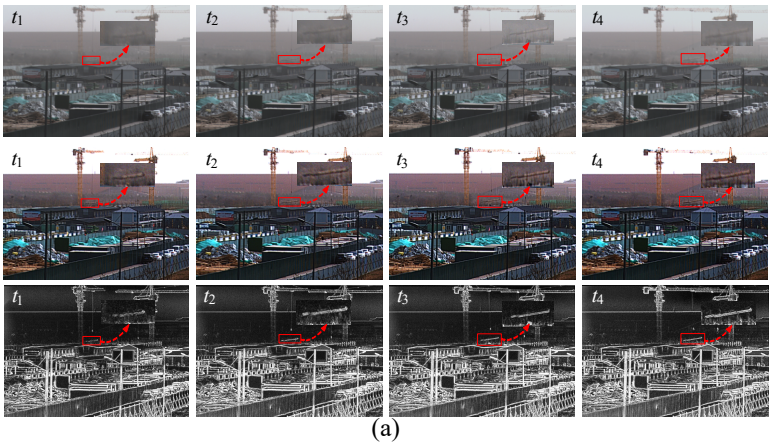
Table 1. NIQE of different image processing schemes.

Methods	Original	DCP	PDCP
NIQE of region1	12.189	6.734	5.010
NIQE of region2	14.562	8.018	5.531
NIQE of region3	14.033	10.091	6.233

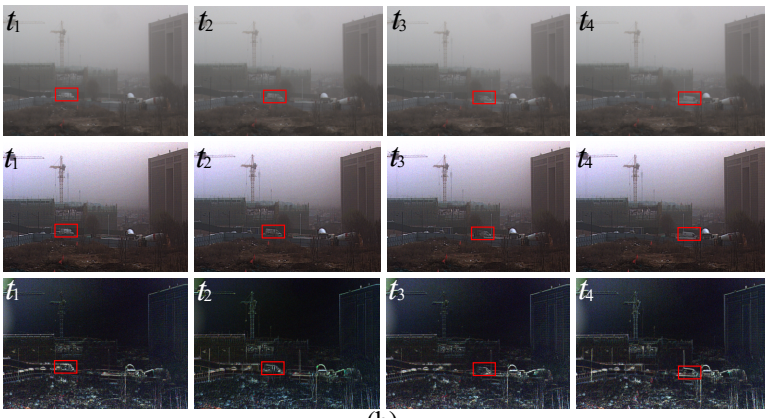
To verify the detection and recognition performance of the polarization imaging system in the experimental scene. We conducted a series of experiments on static and dynamic scenes, as shown in Figures 9 and 10. Figure 9 presents the experimental results for the static scene, and Figure 10 presents the experimental results for the dynamic scene.



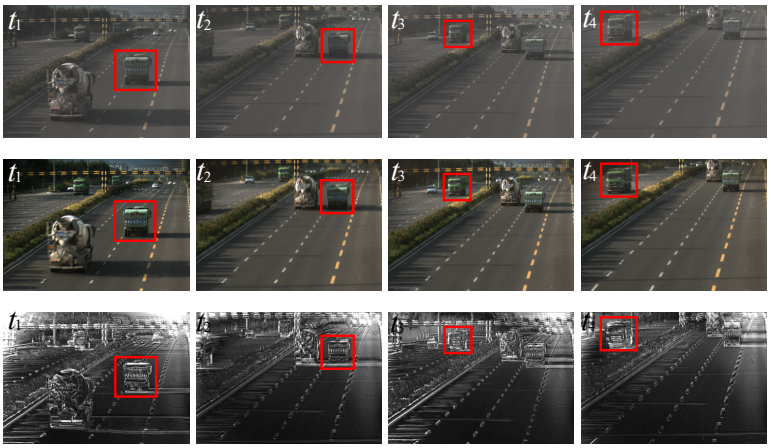
Figure 9. Processing of static scene images. (**a**), Original scene images. (**b**), Scene image after defogging. (**c**), The degree of polarization images.



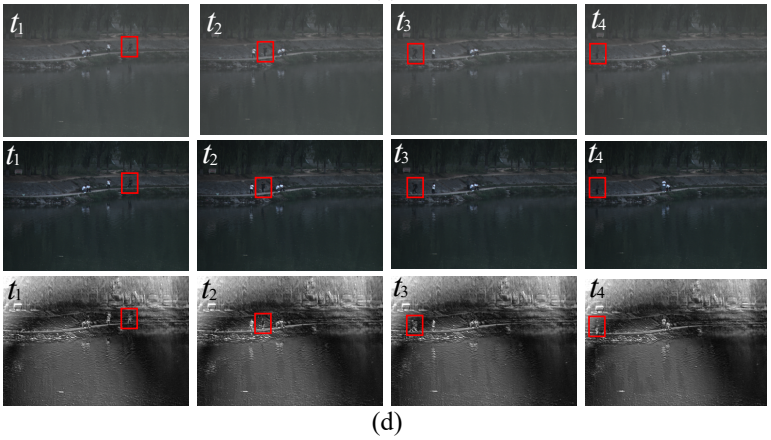
(a)



(b)

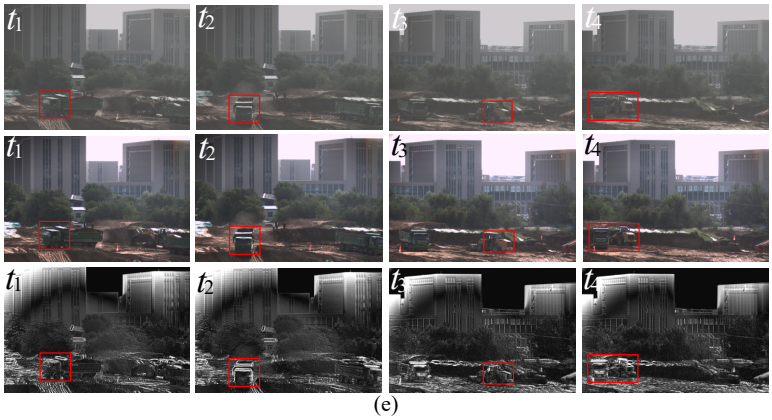


(c)



(d)

Figure 10. *Cont*.



(e)

Figure 10. Processing of dynamic scene images. (**a**–**e**) The comparison results of different scenes at moments t_1–t_4.

By observing Figure 9, it can be seen that the influence of scattering noise on the optical imaging process was effectively suppressed by the dark channel a priori defogging method compared with the original scene image, but the difference between the target and the background was not obvious due to its image representation based on intensity information. However, when polarization information was introduced into the dark channel a prior dehazing image, the target and the background could be clearly identified based on the larger difference in polarization information between them.

The synchronous trigger circuit was adjusted to the closed state while the four polarization channels in the system started to synchronously acquire the polarization images of the same scene, corresponding to 0°, 45°, 90°, and 135°. Next, the scene images at moments of t_1–t_4 were selected as the research objects, as shown in Figure 10. As illustrated in Figure 10a, the dynamic target in a rectangular region of the original scene image is severely affected by a large number of suspended particles, making it difficult to distinguish the target itself and its trajectory. The contrast of the dynamic target in the dehazed scene is obviously improved, but its image expression based on its intensity information makes the difference between the target and the background not clear. As indicated in the degree of polarization images, the object hidden in the tree background on the construction tower crane can be easily identified by the degree of polarization in the image. This is because the degree of polarization image reflects the polarization difference between the target and the background, which enhances the contrast and edge information of the scene image.

Based on these experimental results, the image processing effects of different schemes are quantitatively analyzed by calculating the contrast between the moving object on the tower crane and its background at moments t_1–t_4. The corresponding calculation formula is

$$ICR = |\,(x_i - x_0)/(x_i + x_0)|, \tag{16}$$

where x_i and x_0 represent the average intensity of the moving target itself and the target background region.

The specific contrast calculation results are shown in Table 2. At moments of t_1–t_8, the polarization-based dark channel prior dehazing method increased the contrast of the dynamic target in the rectangular region 1–2 times, respectively, compared to the conventional method. The data in the table also indicate that the proposed method outperforms the traditional dark channel prior dehazing method when the contrast between different targets in the original scene is low, which further demonstrates that the proposed method can effectively overcome the limitations of the traditional scheme.

Table 2. The contrast of the dynamic target within the time interval t_1–t_4.

	Contrast		
Scene/Time	**Original**	**DCP**	**PDCP**
(a)/t_1	0.046	0.104	0.142
(a)/t_2	0.035	0.091	0.217
(a)/t_3	0.033	0.091	0.233
(a)/t_4	0.032	0.087	0.236
(a)/mean value	0.036	0.093	0.207
(b)/t_1	0.155	0.336	0.411
(b)/t_2	0.104	0.271	0.307
(b)/t_3	0.030	0.211	0.289
(b)/t_4	0.144	0.313	0.402
(b)/mean value	0.108	0.282	0.352
(c)/t_1	0.311	0.528	0.694
(c)/t_2	0.164	0.339	0.607
(c)/t_3	0.159	0.411	0.481
(c)/t_4	0.214	0.379	0.597
(c)/mean value	0.212	0.414	0.594
(d)/t_1	0.093	0.166	0.270
(d)/t_2	0.120	0.163	0.183
(d)/t_3	0.097	0.139	0.310
(d)/t_4	0.085	0.091	0.216
(d)/mean value	0.122	0.140	0.244
(e)/t_1	0.288	0.361	0.459
(e)/t_2	0.339	0.627	1.088
(e)/t_3	0.151	0.279	0.341
(e)/t_4	0.197	0.406	0.835
(e)/mean value	0.244	0.418	0.795

Results in Figure 8 are used again to further demonstrate the advantages of polarization information in the identification of targets, which are normalized by mapping it to the range of 0 to 1. The comparisons among direct imaging, dark channel prior and polarization-based dark channel prior, are shown in Figure 11a–c. The red dashed in Figure 11a–c represents the px position corresponding to scene image. The blue and green curves in Figure 11d correspond to the normalized light intensity distribution at the red dashed line position in Figures 11a and 11b, respectively, and the red curve corresponds to the degree of polarization distribution at the red dashed line position in Figure 11c.

The curves of the scene images after dehazing by the dark channel prior are more jittery than those of direct imaging, which means the enhancement of image contrast. In addition to eliminating the influence of scattering noise on the optical imaging process, this method still makes it difficult to distinguish different objects with similar reflectance characteristics. The degree of polarization-encoded information fluctuates more intensely at different pixel positions than that of the intensity information, and the target information representation in the range of 400–600 px positions is more obvious. This result indicates that polarization contains rich information about objects, which can accurately highlight detail features and is conducive to target recognition.

The above results demonstrate that the polarization-based dark channel prior dehazing method has the best characterization capability for the target. However, the research on the polarization information in the above scene images is based on the R, G, and B channels. The polarization characteristics of the object are closely related to the spectrum; therefore, it is necessary to further analyze the intensity of the polarization information in different color channels. Figure 12a–c,e,f provides the RGB channels of the dehazed scene image and the polarization degree image, respectively. The contrast of regions 1–2 is used to quantitatively describe the polarization recognition effect differences of different color channels.

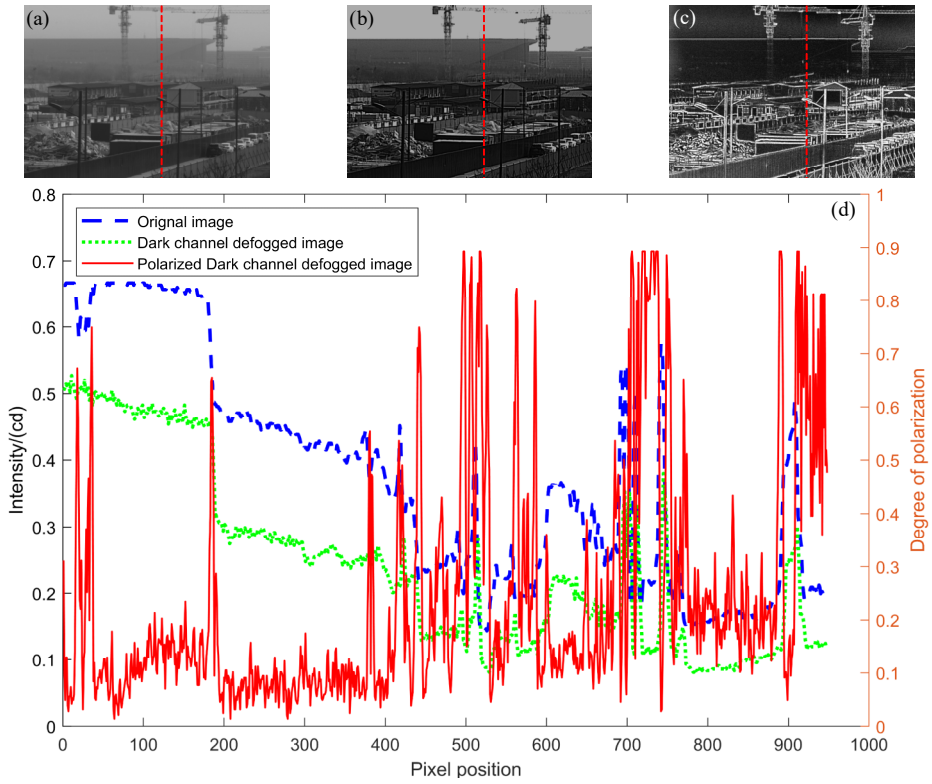


Figure 11. Comparison of light intensity image and polarization image. (**a**) Original scene image. (**b**) Dark channel prior to dehazing the scene image. (**c**) Polarization-based dark channel prior to dehazing the scene image. (**d**) Characterization capabilities of different programs.

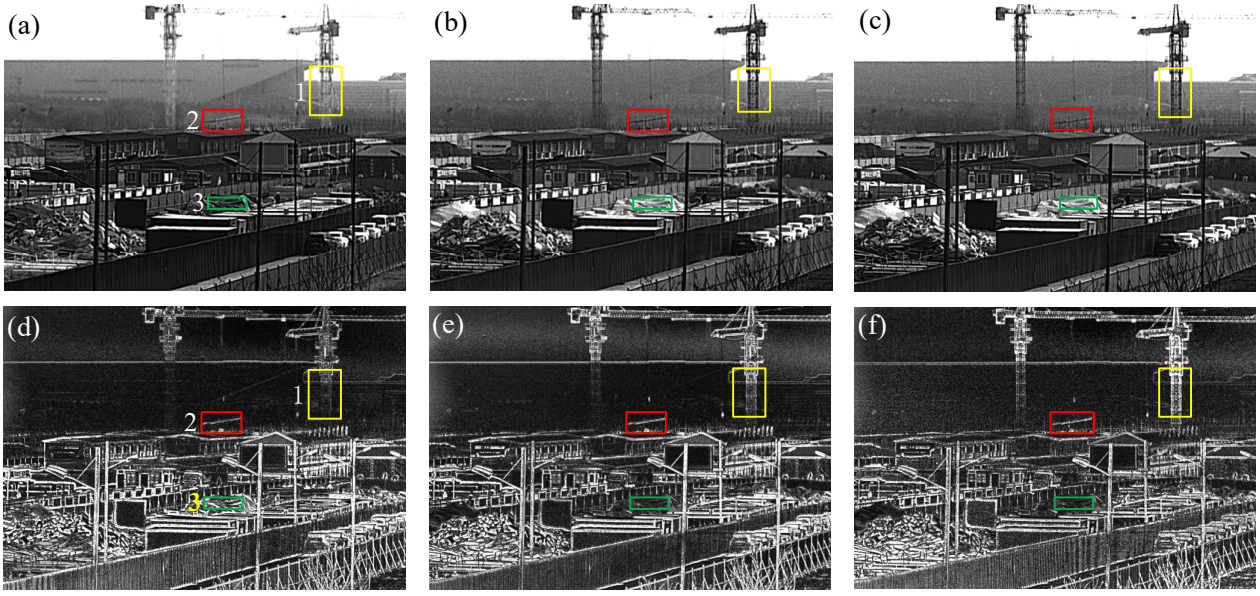


Figure 12. Images of different color channels. Dehazed scene image in the (**a**) R channel, (**b**) G channel, and (**c**) B channel. The degree of polarization image in the (**d**) R channel, (**e**) G channel, and (**f**) B channel.

Table 3 shows the contrast of the polarization RGB image of regions 1–2, and the results show that the contrast of regions 1 and 2 is the highest in the B channel of the polarization degree image.

Table 3. The contrast of polarized images of different color channels.

	Contrast		
Region	**Channel R**	**Channel G**	**Channel B**
1	0.097	0.386	0.614
2	0.123	0.243	0.318

This is due to the following physical reasons: the light intensity distributions of the target in regions 1 and 2 are weak in the B color channel, and the surface is relatively smooth, which reduces the degree of diffuse reflection. Therefore, the degree of polarization in the channel is large; the corresponding dataset is shown in Table 4. The bluish gauze in region 3 of the scene is reflecting more blue light components in the process of propagation, which results in an increase in the number of diffuse reflections on its surface; thus, the image in the B channel shows an increased degree of depolarization.

Table 4. Polarization information in different regions.

	Polarization Information Record		
Region	**Channel R**	**Channel G**	**Channel B**
1	0.169	0.264	0.443
2	0.158	0.192	0.205
3	0.205	0.117	0.106

The main focus of this chapter is on the performance of the polarization imaging system for detecting and recognizing dynamic targets in foggy conditions. The polarization imaging system is used to acquire the original images of each polarization channel for a dynamic target scene within a certain time interval. The degree of polarization of the images is obtained by dehazing the original images using the dark channel prior method and by integrating the polarization information with the dehazed images. The specific regions of interest of the above three sets of images are compared and quantitatively analyzed, and the merits and demerits of different approaches for target representation ability are evaluated. Moreover, by investigating the enhancement effect of different color channel images on target features, the relationship between polarization features and spectrum is thoroughly analyzed.

5. Conclusions

This paper proposes a polarization-based dark channel prior dehazing method to improve the efficiency of detecting and characterizing foggy targets. The main contributions of this paper are that the proposed method can effectively detect the target hidden in the background with similar reflectivity by using a combination of intensity and polarization. Moreover, a polarization imaging system with a split-amplitude structure is designed and built to enable real-time acquisition of transient scene targets. In the next step, we will attempt to carry out secondary development of the software architecture currently owned by the system, aiming to achieve real-time acquisition of the target scene while processing the target in real time. In addition, we intend to fuse the dehazed intensity image and the polarization image to shorten the time for target recognition and enhance the detection efficiency.

Author Contributions: J.G. proposed the original idea. H.S. conducted the experiments and designed the instrument. M.M. and N.W. performed the experiments. Y.H. and L.Z. collected and analyzed the data. H.S. wrote the manuscript. H.S. and Y.C. reviewed and edited the manuscript. All authors have read and agreed to the published version of the manuscript.

Funding: This work was supported by the Fundamental Research Program of Shanxi Province (20210302124702), the National Natural Science Foundation of China (62005251, 62305237), and the Central Guidance on Local Science and Technology Development Fund of Shanxi Province (YDZJSX2022A031).

Data Availability Statement: Data sharing is not applicable due to privacy restrictions.

Conflicts of Interest: The authors declare no conflict of interest.

References

1. Horvath, H. Basic optics, aerosol optics, and the role of scattering for sky radiance. *J. Quant. Spectrosc. Ra.* **2014**, *139*, 3–12. [CrossRef]
2. Raikwar, S.C.; Tapaswi, S. An improved linear depth model for single image fog removal. *Multimed. Tools Appl.* **2018**, *77*, 19719–19744. [CrossRef]
3. Xie, Y.; Ning, L.; Wang, M.; Li, C. Image enhancement based on histogram equalization. *J. Phys. Conf. Ser.* **2019**, *1314*, 012161. [CrossRef]
4. Gao, J.; Wang, B.; Wang, Z.; Kong, F. A wavelet transform-based image segmentation method. *Optik* **2020**, *208*, 164123. [CrossRef]
5. Wang, J.B.; He, N.; Zhang, L.L.; Lu, K. Single image dehazing with a physical model and dark channel prior. *Neurocomputing* **2015**, *149*, 718–728. [CrossRef]
6. Lee, S.; Yun, S.; Nam, J.H.; Won, C.S.; Jung, S.W. A review on dark channel prior based image dehazing algorithms. *EURASIP J. Image Video Process.* **2016**, *2016*, 4. [CrossRef]
7. Peng, Y.T.; Cao, K.; Cosman, P.C. Generalization of the dark channel prior for single image restoration. *IEEE Trans. Image Process.* **2018**, *27*, 2856–2868. [CrossRef]
8. Song, Y.; He, Z.; Qian, H.; Du, X. Vision transformers for single image dehazing. *IEEE Trans. Image Process.* **2023**, *32*, 1927–1941. [CrossRef]
9. Zhou, C.; Teng, M.; Han, Y.; Xu, C.; Shi, B. Learning to dehaze with polarization. *NIPS* **2021**, *34*, 11487–11500.
10. Wu, M.; Zhang, C. Optimizing polarization dehazing. *Mod. Phys. Lett. B* **2021**, *35*, 2150332. [CrossRef]
11. Li, X.; Liu, F.; Han, P.; Wei, Y.; Zhao, D.; Shao, X.; Zhao, X. Research on polarization dehazing through the coaxial and multi-aperture polarimetric camera. *OSA Contin.* **2019**, *2*, 2369–2380. [CrossRef]
12. Zhang, W.; Liang, J.; Wang, G.; Zhang, H.; Fu, S. Review of passive polarimetric dehazing methods. *Opt. Eng.* **2021**, *60*, 030901. [CrossRef]
13. Tuchin, V.V. Polarized light interaction with tissues. *J. Biomed. Opt.* **2016**, *21*, 071114. [CrossRef]
14. Cheng, S.C.; Lee, K.C.; Huang, C.W. Radar target recognition by polarization-diversity RCS including random effects. *Int. J. Appl. Electron.* **2015**, *47*, 939–949. [CrossRef]
15. Dubreuil, M.; Delrot, P.; Leonard, I.; Alfalou, A.; Brosseau, C.; Dogariu, A. Exploring underwater target detection by imaging polarimetry and correlation techniques. *Appl. Opt.* **2013**, *52*, 997–1005. [CrossRef]
16. Ma, T.; Hu, X.; Lian, J.; Zhang, L. A Novel Calibration Model of Polarization Navigation Sensor. *IEEE Sens. J.* **2015**, *15*, 4241–4248. [CrossRef]
17. Chen, Z.; Zhang, D.; Xu, Y.; Wang, C.; Yuan, B. Research of polarized image defogging technique based on dark channel priori and guided filtering. *Procedia Comput. Sci.* **2018**, *131*, 289–294. [CrossRef]
18. Jia, Q.; Hou, Q. Haze Removal Using Polarization Dark Channel Prior with Applications to Marine Target Enhancement. *Opt. Express* **2019**, *27*, 33765–33782.
19. Meng, Y.; Liu, C.; Wang, X.; Zhou, Z. Polarization Dehazing with Dual Images Based on Dark Channel Quartering. In *Fourier Transform Spectroscopy*; Optica Publishing Group: Washington, DC, USA, 2021; paper ID JTu5A. [CrossRef]
20. Narasimhan, S.G.; Nayar, S.K. Vision and the atmosphere. *Int. J. Comput. Vision* **2002**, *48*, 233–254. [CrossRef]
21. He, K.; Sun, J.; Tang, X. Single image haze removal using dark channel prior. *IEEE. Pattern Anal.* **2010**, *33*, 2341–2353.
22. Siegman, A. Fresnel reflection, Lenserf reflection and evanescent gain. *Opt. Photonics News* **2010**, *21*, 38–45. [CrossRef]
23. Lu, X.; Jin, W.; Li, L.; Wang, X.; Qiu, S.; Liu, J. Theory and analysis of a large field polarization imaging system with obliquely incident light. *Opt. Express* **2018**, *26*, 2495–2508. [CrossRef] [PubMed]
24. Śliwa, R.E.; Pawłowska, B.; Balawender, T.; Zwolak, M. Extrusion of Lightweight Aluminum and Magnesium Alloys Structures for Aviation Applications. *Key Eng. Mater.* **2022**, *926*, 523–536. [CrossRef]
25. Xu, M.J.; Gbur, G.; Visser, T.D. Generalization of Malus' law and spatial coherence relations for linear polarizers and non-uniform polarizers. *Opt. Lett.* **2022**, *47*, 5739–5742. [CrossRef]

Disclaimer/Publisher's Note: The statements, opinions and data contained in all publications are solely those of the individual author(s) and contributor(s) and not of MDPI and/or the editor(s). MDPI and/or the editor(s) disclaim responsibility for any injury to people or property resulting from any ideas, methods, instructions or products referred to in the content.